# DISTINCT ELEMENT MODELING OF THE DYNAMIC RESPONSE OF A ROCKING PODIUM TESTED ON A SHAKE TABLE

## Daniele Malomo<sup>1</sup>, Anjali Mehrotra<sup>2</sup>, and Matthew J. DeJong<sup>3</sup>

<sup>1</sup>Department of Civil Engineering and Applied Mechanics, McGill University, Montréal, Canada <sup>2</sup>ISISE, Department of Civil Engineering, University of Minho, Guimarães, Portugal <sup>3</sup>Department of Civil and Environmental Engineering, University of California, Berkeley, United States

A blind prediction contest was organized to evaluate the ability of different modeling approaches to simulate the seismic rocking response of a full-scale four-column podium structure. The structure was tested on a shake table, and was subjected to two bidirectional ground motion ensembles comprising 100 synthetic records each. This short communication presents the main assumptions and results from the model, developed using the Distinct Element Method (DEM), which provided the second-best prediction of the experimental results. A comparison of the model predictions and the experimental results demonstrates that the numerical model was generally able to reproduce the large displacements induced by the more intense ground motion ensemble, while tending to overestimate the displacements of the less intense earthquake ensemble. This overestimation of the response was reduced through the inclusion of damping in the system. However, the addition of damping greatly increased the solve time which is problematic for a competition, and in the case of the more intense ground motion ensemble also resulted in an underprediction of the maximum response of the structure.

#### **KEYWORDS**

Rocking, dynamic analysis, shake-table test, Distinct Element Method, blind prediction contest

#### INTRODUCTION

A full-scale four-column rocking podium structure, comprised of an aluminium slab supported on four cylindrical structural steel columns, was tested under artificially-generated bi-directional seismic excitations using a 6-dof shaking table. The specimen was designed at ETH Zurich, while the shake table tests were conducted at the Earthquake and Large Structures (EQUALS) Laboratory of the University of Bristol, UK, under the SERA transnational access project "3DROCK: Statistical Verification and Validation of 3D Seismic Rocking Motion Models". For details regarding the experimental configuration and test-set up of the prototype (including a description of the signals applied to the shake-table), which have been explicitly reproduced numerically, the reader is directed to Vassiliou et al (2020).

In this modeling exercise, a numerical model based on the Distinct Element Method (DEM) (Cundall 1971), and implemented in 3DEC (Itasca Consulting Group Inc. 2013), was developed with the objective of predicting the dynamic response of the specimen briefly described above and depicted in Figure 1. The ability of DEM to model large block displacements and the opening and closing of joints makes it particularly useful for modeling rocking motion. It has previously been applied with satisfactory results to the analysis of rocking structures such as single rigid blocks (Peña et al. 2007, DeJong 2009), walls (Al Shawa et al. 2012), spires (DeJong and Vibert 2012), arches (De Lorenzis et al. 2007) and columns (Papantonopoulos et al. 2002; Psycharis et al. 2003).

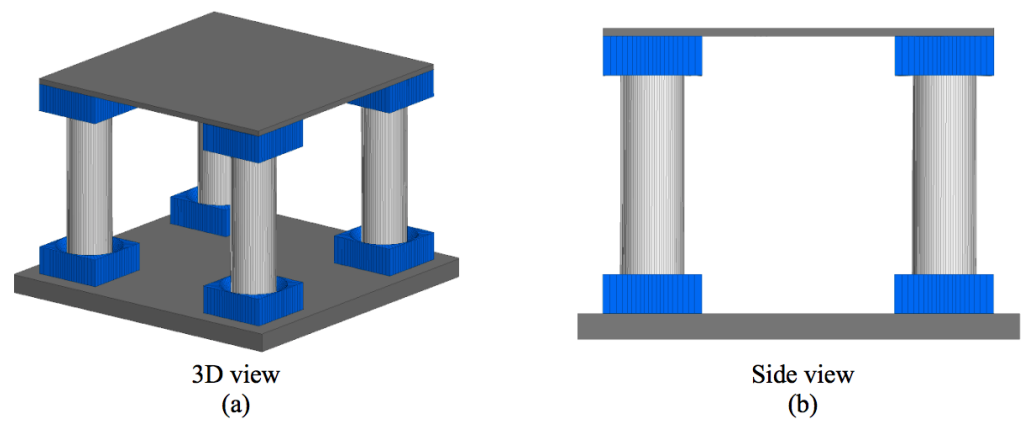


Figure 1 (a) 3D and (b) elevation view of the proposed discrete element model.

#### **METHODOLOGY**

In the case of the proposed model, rigid blocks, in contact with each other through nonlinear interface springs with zero thickness, were used to represent both the columns and the foundation/top slabs, as well as the cylindrical restraints. Material densities were specified as 8000 kg m<sup>-3</sup> and 2700 kg m<sup>-3</sup> for the structural steel and aluminium elements respectively. Each rigid block is characterised by six degrees of freedom; when contact is detected, faces are triangulated to create sub-contacts, located at the element vertices. Normal  $(k_n)$  and shear  $(k_s)$  stiffnesses were assigned at sub-contacts between solid elements, as depicted in **Errore. L'origine riferimento non è stata trovata.** In the elastic range, under a shear-compression biaxial stress-state, the joint behavior is governed by:

$$\Delta \sigma_n = k_n \Delta u_n \tag{1}$$

$$\Delta \tau_{\rm s} = k_{\rm s} \Delta u_{\rm s} \tag{2}$$

where  $\sigma_n$  and  $\tau_s$  are the normal and shear stresses respectively,  $k_n$  and  $k_s$  are the normal and shear joint stiffnesses, and  $\Delta u_n$  and  $\Delta u_s$  correspond to differential displacements (see Figure 2).

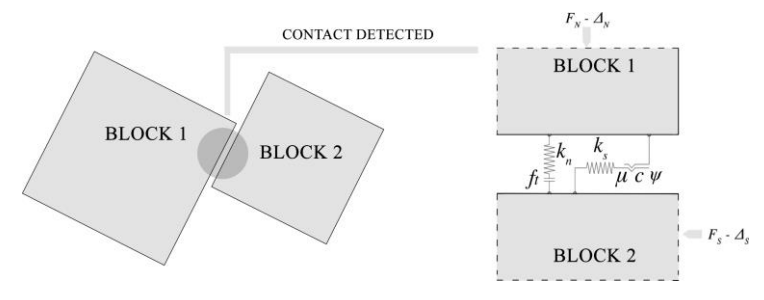


Figure 2 Graphical representation of the contact between adjacent blocks (adapted from Malomo et al (2019)).

Cohesive-frictional sliding joints between columns and restraints were modeled using a simplified Mohr-Coulomb criterion with tension cut-off. The maximum local shear resistance is given by Equation (3). The cohesion parameter, c, is set to zero right after reaching the maximum shear strength  $F_{S,max}$ , thus neglecting any post-peak softening branch. This results in a residual capacity  $F_{S,res}$  governed by the acting vertical force  $F_{N,max}$  and the selected friction angle  $\phi$  (Equation (4)).

$$F_{S,max} = c + F_{N,max} tan\phi (3)$$

$$F_{S.res} = F_{N.max} tan\phi \tag{4}$$

For the majority of discrete methods (e.g. Meguro and Tagel-Din 2000; Rafiee et al. 2008), loading-reloading modelling is not directly incorporated in the formulation. In the DEM framework, the representation of stiffness and strength degradation phenomena depends on the number of springs that have failed in tension, whose resistance is set to zero in the subsequent steps, as well as on both the extent and location of joint slip, i.e. where  $F = F_{S,res}$ . Normal displacements due to dilation phenomena  $u_{n,dil}$ , which take place only at the onset of shear failure, can be accounted for by introducing the parameter  $\psi$ , i.e. iteratively correcting the total normal force  $F_{N,tot}$  acting at the joint level as a function of the direction of shearing until the limiting shear displacement ( $ul_{s,dil}$ ) is reached:

$$\Delta u_{n.dil} = \Delta u_s tan \psi \tag{5}$$

$$F_{N,tot} = k_n \Delta u_n + k_n \Delta u_s \tan \psi \tag{6}$$

In this exercise, cohesion (c), tensile strength ( $f_t$ ) and dilation ( $\psi$ ) were set to zero from the beginning of the analysis. Thus, the interface frictional resistance in the model only relies on the friction angle  $\phi$ , which was set to 11.3° based on an assumed coefficient of friction of 0.2 (Zhang et al. 2008). On the other hand, failures induced by high compressive stress localization were neglected. Finally, both  $k_n$  and shear  $k_s$  were set equal to 1e9 Pa/m, representing the smallest iteratively-calibrated value beyond which interpenetration phenomena among adjacent elements occurred. Ideally, only stiffness proportional damping would be employed, with mass proportional damping set to zero (DeJong 2009). However, stiffness proportional damping significantly decreases the timestep, which greatly increased computation time. For the blind prediction competition, a long-time step was problematic since 200 time-history simulations were required. As a result, no numerical damping was specified, i.e. both mass and stiffness proportional damping were set to zero. The assumption of no damping can be effective for dynamic simulations (Psycharis et al. 2003), and is particularly reasonable for this structure where cone-shaped constraints

keep the columns in place and prevent vibration displacements, which can be unrealistically predicted in simulations when high frequency damping is neglected (DeJong, 2009). Nevertheless, damping is a very important parameter in DEM, and the effect of this no damping assumption is also evaluated for a few of the time history simulations. Moreover, given that in the employed computational platform it is presently not possible to model curved solids, the specimen geometry was slightly simplified. Specifically, all circular cross-sections were discretized into *n*-sided regular polygons, with an investigation conducted into the number of sides required to accurately capture the cross-sectional area of the columns. Consequently, the circular cross-sections were replaced with 80-segment polygons which were then joined together, forming a single rigid element as illustrated by Figure 3(a). This results in approximately 160 springs per contact surface (80 on the inner surface and 80 on the outer surface, see Figure 3(b) where springs are coloured in black).

In terms of boundary conditions, and with reference to Figure 1 and Figure 3, the blue conical restraints, the dark grey top or bottom slabs and the red pegs that were installed to prevent overturning, were joined together, allowing no relative displacement between these parts. The ground motion was simulated by specifying a velocity time history to the foundation. Finally, in order to further reduce computational expense, each of the experimentally-employed signals were truncated at different time instants, depending on their properties, with the objective of capturing the most destructive significant 20 seconds of the ground motion. These truncated records were then applied to the model simultaneously in the *x* and *y* directions.

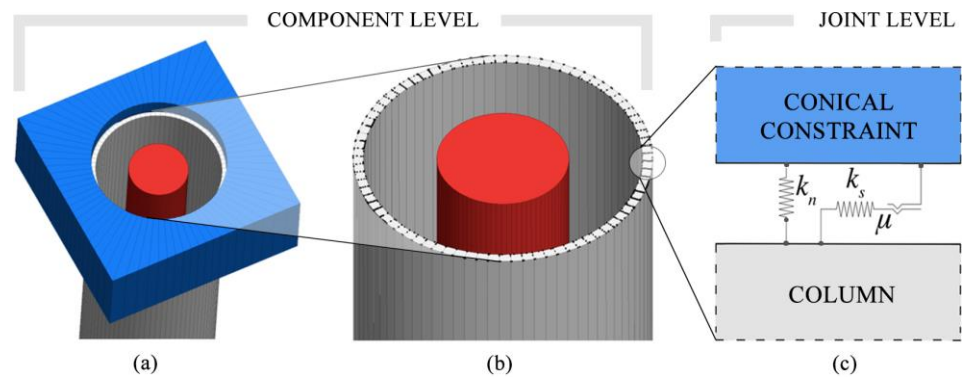


Figure 3 (a) proposed discretization of circular cross-sections, identification of interface springs at both (b) component and (c) joint level

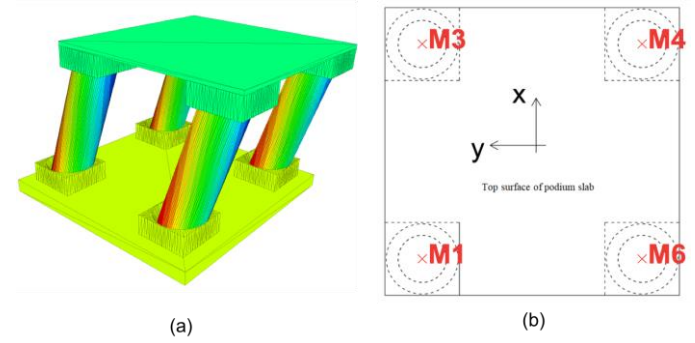


Figure 4 (a) Sample deformed configuration of the rocking podium and (b) points at which the displacements were monitored (adapted from Vassiliou et al (2020)).

### **RESULTS**

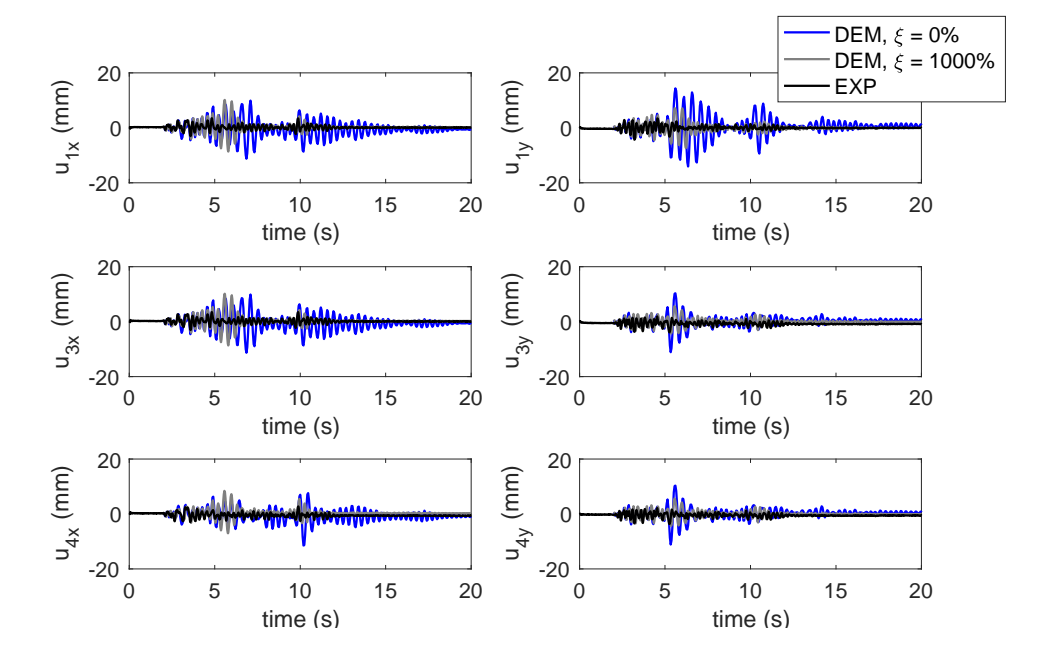
The adopted simplified modeling strategy made it possible for all 200 simulations to be conducted in a reasonable time-frame. For each run, the relative displacements of the slab at the top of the podium were monitored at four points (M1-M6) as illustrated by Figure 4b. The contest rules required the maximum absolute average displacement (MAAD, denoted by u) to be submitted for each run, which was then computed using Equation 7, where  $u_{ix}$  and  $u_{iy}$  are the horizontal displacements recorded at each of the points  $M_i$  (Figure 4b) in the x and y directions. Comparative time-histories of these displacements can be found in Figures 5 and 6 for the El Centro and Chi-Chi ground motion ensembles respectively:

$$u = \max_{t} \left( abs \left( \frac{\sqrt{u_{1x}(t)^{2} + u_{1y}(t)^{2}} + \sqrt{u_{3x}(t)^{2} + u_{3y}(t)^{2}} + \sqrt{u_{4x}(t)^{2} + u_{4y}(t)^{2}} + \sqrt{u_{6x}(t)^{2} + u_{6y}(t)^{2}}}{4} \right) \right)$$
(7)

As the Figure 5 illustrates, for record #1 of the El Centro ground motion ensemble, the undamped numerical model predicted larger displacements than those recorded in the experimental tests, resulting in an overprediction of the MAAD by a factor of 3.5. Re-running the analysis with 1000% stiffness-proportional damping applied at the impact frequency of the system (1100 Hz) lead to an overall reduction of the response, but still resulted in an overprediction of the MAAD by a factor of 2.8. A better correlation was observed in the case of the Chi-Chi ensemble, with the undamped DEM model capturing the experimental response fairly well for the first few cycles of ground motion (shown in Figure 6 for record #7), and only overestimating the MAAD by a factor of 1.2. This is due to the higher intensity of the Chi-Chi ground motion, which induced considerably larger displacements in the structure. The numerical model was still on the conservative side, even predicting overturning in a few cases (i.e. simulations 31, 64, 68 and 96 of the Chi-Chi ensemble), although in reality the specimen did not collapse. In this case, introducing damping into the system did not appear to significantly reduce the response, with the exception of the peak displacement between 11-13 seconds, which was underestimated and thus resulted in an underprediction of the MAAD by a factor of 0.84. In general, the proposed (i.e. undamped) DEM model was found to be capable of reproducing the large displacements induced by the more intense Chi-Chi ensemble, but tended to overestimate the smaller displacements of the El Centro ground motion. This was observed both through a motion-by-motion comparison of the experimental and numerical MAAD responses (Figure 7, with the numerical model on average overpredicting the MAAD by a factor of 1.56 and 1.14 for the El Centro and Chi-Chi ensembles respectively), as well as a comparison of their CDF plots (see Figure 8; experimental values from Vassiliou et al (2020)). The performance of the different modelling approaches was finally evaluated using the Kolmogorov-Smirnov (K-S) distance, which measures the error as the maximum vertical distance between the experimental and numerically-obtained MAAD CDFs. In the case of the El Centro ensemble, the K-S distance for the proposed model was found to be 0.36 (rank 5), while for the more intense Chi-Chi ensemble, the K-S distance was found to be 0.06 (rank 1, with just over half the error of the two trailing teams, both of which recorded a K-S distance of 0.11), resulting in an average K-S distance of 0.21 and an overall rank of 2.

#### **CONCLUSIONS**

In this paper, the development and predictions of a numerical model based on the Distinct Element Method (DEM) used for reproduction of the 3D wobbling response of a full-scale rocking podium structure are presented and discussed. The structural components of the podium were modelled as rigid blocks and the connections between them as nonlinear springs with no tensile strength or cohesion. No damping was used in the analyses, while the input ground motions were truncated to reduce computational expense. These simplified assumptions made it possible to obtain results in a reasonable timeframe, which is usually challenging when employing these types of computational techniques. A comparison of the numerical predictions with the experimental response revealed the proposed DEM model to generally be capable of reproducing the large displacements induced by the more intense Chi-Chi ensemble (with a relatively good agreement observed for the first few cycles of motion), while overestimating the smaller displacements of the El Centro ground motion suite. Overall, the model was found to rank 2<sup>nd</sup> overall, evaluated based on the average Kolmogorov-Smirnov distance between the experimental and numerical maximum absolute average displacement (MAAD) CDF plots for both ground motion ensembles.



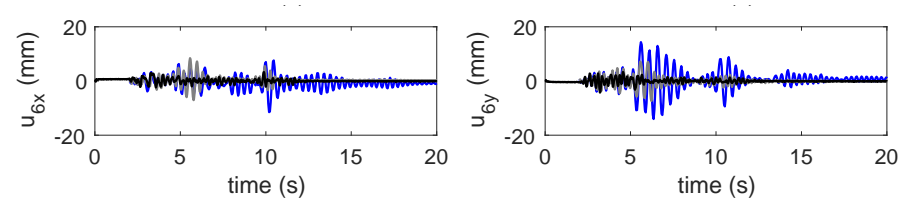


Figure 5 Numerical and experimental displacement time-histories recorded in the structure for record #1 of the El Centro ensemble ( $u_{\text{EXP}} = 3.99 \text{ mm}$ ,  $u_{\text{DEM}, 0\%} = 14.1 \text{ mm}$  and  $u_{\text{DEM}, 1000\%} = 11.2 \text{ mm}$ ).

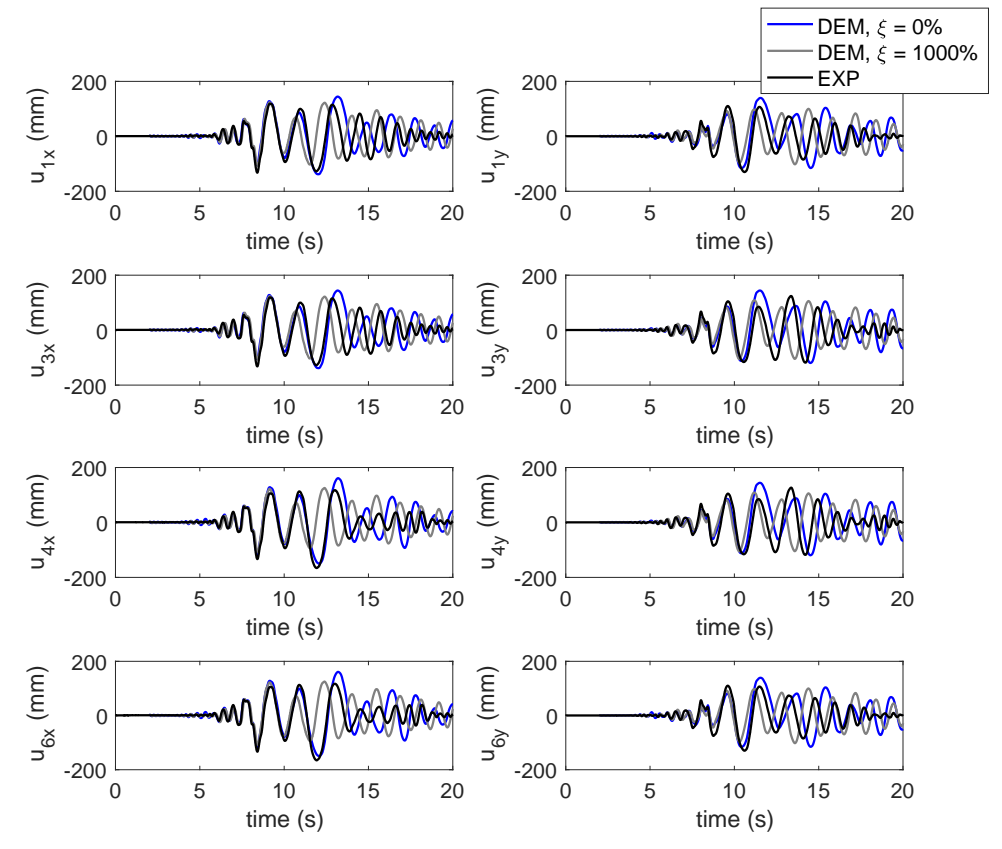


Figure 6 Numerical and experimental displacement time-histories recorded in the structure for record #7 of the Chi-Chi ensemble ( $u_{\text{EXP}} = 150.6 \text{ mm}$ ,  $u_{\text{DEM}, 0\%} = 175.4 \text{ mm}$  and  $u_{\text{DEM}, 1000\%} = 126.8 \text{ mm}$ ).

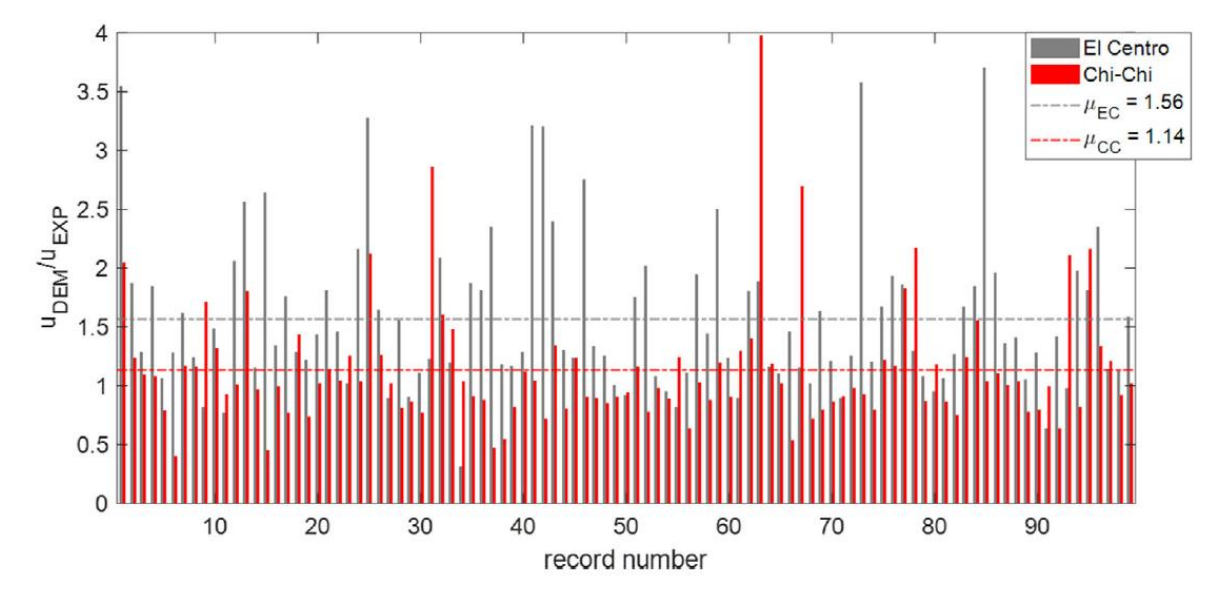


Figure 7 Motion-by-motion experimental vs numerical (undamped) MAAD (u) for both ground motion ensembles.

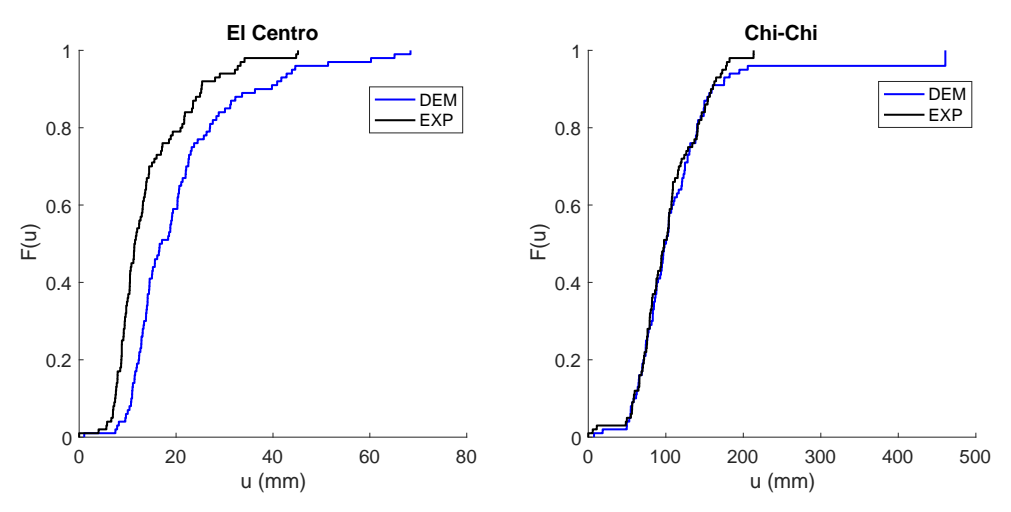


Figure 8 Motion-by-motion comparison of the experimental and numerical (undamped) MAAD (u)

#### REFERENCES

Vassiliou MF, Broccardo M, Cengiz C, Dietz M, Dihoru L, Gunay S, Mosalam K, Mylonakis G, Sextos A and Stojadinovic B. Shake Table Testing of a Rocking Podium: Results of a Blind Prediction Contest. Earthquake Engineering & Structural Dynamics 2020; 1-20.

Al Shawa O, de Felice G, Mauro A and Sorrentino L. Out-of-plane seismic behaviour of rocking masonry walls. Earthquake Engineering & Structural Dynamics 2012; 41(5): 949-968.

Cundall, PA. A computer model for simulating progressive large-scale movements in blocky rock systems. Proceedings of the Symposium of the International Society of Rock Mechanics, Nancy, France, 1971, No. 8.

DeJong MJ. Seismic Assessment Strategies for Masonry Structures. PhD Thesis, Massachusetts Institute of Technology, Cambridge, USA, 2009.

DeJong MJ and Vibert C. Seismic response of stone masonry spires: Computational and experimental modeling. Engineering Structures 2012; 40: 566-574.

De Lorenzis L, DeJong MJ and Ochsendorf J. Failure of masonry arches under impulse base motion. Earthquake Engineering & Structural Dynamics 2007; 36(14); 2119-2136.

Itasca Consulting Group Inc. 3DEC. Three Dimensional Distinct Element Code. 2013.

Malomo D, DeJong MJ, Penna A. Distinct element modelling of the in-plane cyclic response of URM walls subjected to shear-compression. Earthquake Engineering & Structural Dynamics 2019; 48(12); 1322-1344.

Meguro K, Tagel-Din H. Applied element method for structural analysis: Theory and application for linear materials. Structural Engineering/Earthquake Engineering 2000, 17(1).

Papantonopoulos C, Psycharis IN, Papastamatiou DY, Lemos JV and Mouzakis HP. Numerical prediction of the earthquake response of classical columns using the distinct element method. Earthquake Engineering & Structural Dynamics 2002; 31:1699-1717.

Peña F, Prieto F, Lourenço PB, Campos Costa A and Lemos JV. On the dynamics of rocking motion of single rigid-block structures. Earthquake Engineering & Structural Dynamics 2007; 36:2383-2399.

Psycharis IN, Lemos JV, Papastamatiou DY, Zambas C and Papantonopoulos C. Numerical study of the seismic behaviour of a part of the Parthenon Pronaos. Earthquake Engineering & Structural Dynamics 2003; 32(13): 2063–2084.

Rafiee A, Vinches M and Bohatier C. Modelling and analysis of the Nìmes arena and the Arles aqueduct subjected to a seismic loading using the Non-Smooth Contact Dynamics method. Engineering Structures 2008; 30(12): 3457–3467.

Zhang PC, Nagae T, McCormick J, Ikenaga M, Katsuo M and Nakashima M. Friction-based sliding between steel and steel, steel and concrete, and wood and stone. 14<sup>th</sup> World Conference on Earthquake Engineering, Beijing, China, 2008.